CONF-801099--1

SYSTEM FOR CONTROL OF ELECTROSLAG CASTING IN A COLLAR MOLD*

J. W. McEnerney, B. R. Dewey,† J. T. Hutton, and S. A. David
Metals and Ceramics Division
Oak Ridge National Laboratory
Oak Ridge, Tennessee 37830

ABSTRACT

This report describes the initial development of an electroslag casting control system at Oak Ridge National Laboratory The main emphasis of our work and the results reported herein deal with the attempts to develop techniques for locating and controlling the liquid slag-metal interface. Thermocouples embedded in the mold wall provide a simple but accurate means for locating the interface.

INTRODUCTION

The electroslag casting (ESC) process can produce ingots with graded composition, as would be useful in transition joints between type 316 stainless steel and 2 1/4 Cr-1 Mo steel (1). This can be accomplished by melting a composite electrode. We have established an ESC system at Oak Ridge National Laboratory (RNL) to enable us to study fabrication techniques for producing such graded composition ingots. Although we are reporting only work on solid ingots, our system has been designed with the capability for producing hollow ingots. The hollow ingots offer improved structure

*Research sponsored by the Exploratory Studies Program, Oak Ridge National Laboratory, operated by Union Carbide under contract W-7405-eng-26 for the U.S. Department of Energy.

†Professor, Department of Engineering Science and Mechanics, University of Tennessee, Knoxville, Tennessee.

coupled with economic advantage (2-4). Our system is designed for dynamic operation with an ingot being withdrawn from the bottom of a stationary mold.

To produce desirable structures during ESC, one needs to accurately monitor and control key process parameters. During dynamic casting (relative motion between mold and ingot) of hollow or solid ingots, additional critical control of the process is required to maintain the liquid slag-metal interface at a desired location. Therefore, our initial work was aimed at developing a data acquisition and control system (DACS) for real-time control of our ESC operation.

Our system currently utilizes two 1000-A dc constant-potential electroslag welding power supplies, which will be replaced by a single 5000-A ac regulated-current power supply. Because we are using welding power supplies, certain aspects of necessary electrode feed control capability cannot currently be implemented. However, our present equipment has enabled us to develop most aspects of the DACS.

This report describes the development of our system. The main emphasis of our work and the results reported herein deal with the attempts to develop techniques for locating and controlling the liquid slag-metal interface.

BRIEF DESCRIPTION OF ESC PROCESS

The fundamentals of electroslag refining or casting are adequately described by Duckworth and Hoyle (5). Figure 1 schematically illustrates the ESC process as currently implemented at ORNL. As shown, current is passed through a consumable electrode, which is immersed in a molten slag bath. The flow of current through the slag causes resistance heating. As the electrode enters the bath, droplets melt off and pass through the slag to form a molten pool. A water-cooled copper mold is used to extract heat and freeze the liquid metal pool. Since the liquid slag solidifies before the liquid metal, a solid slag skin forms around the outer surface of the ingot. This skin and subsequent air gap formation provide a thermal barrier for heat transfer between the solidifying ingot and the mold wall. During operation, the ingot is withdrawn from the bottom of the mold. In order to maintain steady-state conditions, the volume of melting electrode must equal the volume of withdrawn ingot.

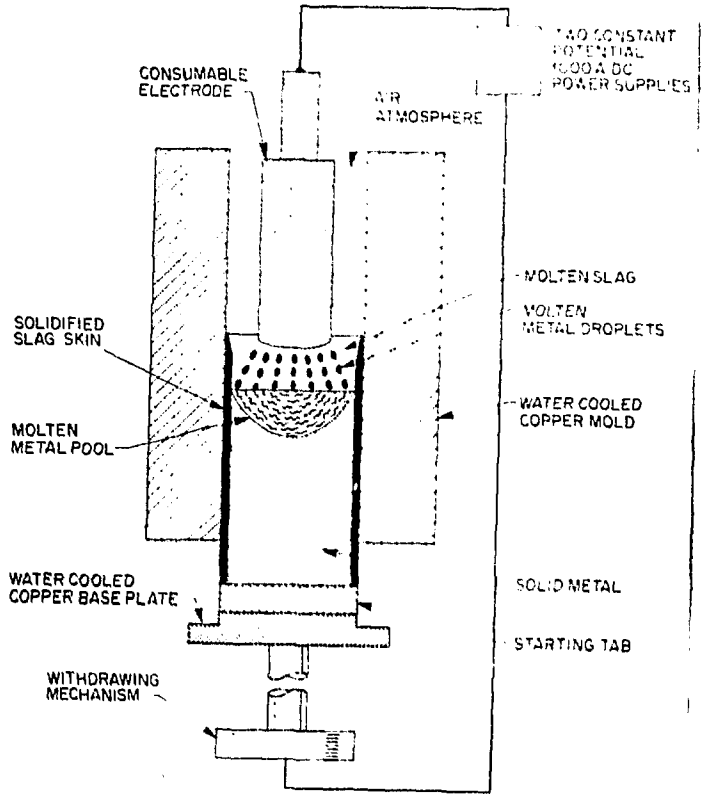

Fig. 1. Electroslag Casting Process as Implemented at ORNL.

DESCRIPTION OF EQUIPMENT

We have designed and assembled our ESC system furnace and control equipment. The electrode feed mechanism on the furnace is driven by a 37-W permanent-magnet dc motor-generator with a solid-state electronic controller capable of remote or manual operation. The motor-generator is operated under speed feedback control in both remote and manual modes. In the remote mode, a 0 to 10-V dc signal can be sent to control the speed set point. In addition, the motor polarity can be remotely reversed to provide the desired motion. The electrode feed mechanism has a maximum feed speed of about 5 mm/s and is typically operated in the range 0.1 to 0.2 mm/s. The water-cooled electrode holder is

spended from a 2.2-kN load cell, which is electrically isolated from the current path. An approximately 1-m-long electrode can be accommodated by the available travel distance. We are currently using 63.5-mm-diam electrodes. However, we plan to use larger diameter electrodes with the bigger power supply. Our current fill ratio (area of electrode to area of mold) of 39% is near the lower end of the normally used range of 40 to 60%.

Figure 2 shows a sketch of our mold. We are currently capable of withdrawing 0.1-m-diam by 0.6-m-long solid ingots. The mold consists of three pairs of cooling water channels spaced 120° apart around a 25.4-mm-thick copper cylinder. The mold is supported by an integral copper flange. The water enters an inlet at the bottom of the mold, flows vertically upward through a 9.5-mm-diam channel, flows circumferentially around the top of the mold through a 9.5- by 9.5-mm channel, and then flows vertically down and out of the mold at the bottom. The water typically flows through the channels at a volume rate of about 1.3×10^{-4} m^3/s. Our

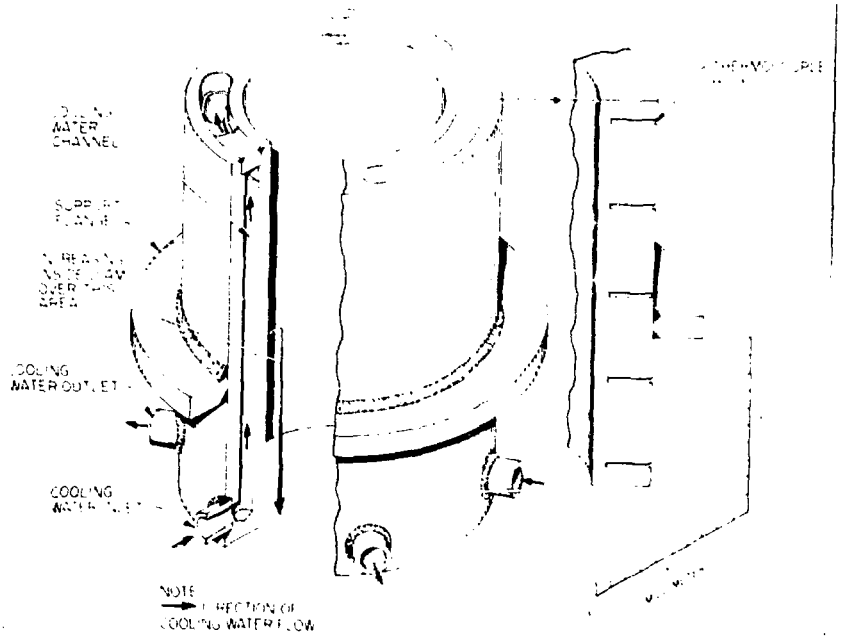

Fig. 2. ORNL Water-Cooled Copper Mold.

particular mold configuration was chosen over one with a continuous water jacket for several reasons. First, we wanted a continuous path through the mold wall for passage of ultrasonic waves, as will be discussed later. In addition, this design also simplified thermocouple penetrations in the mold wall. However, it should be noted that our mold design results in a nonaxisymmetric temperature distribution, as will be shown later by finite-element modeling. Therefore, a mold with a continuous water jacket may be used in the future.

An array of five thermocouples is embedded in the mold wall in a vertical plane 15° from one of the inlet channels. Each thermocouple location corresponds to a node in the finite-element mesh, to be shown later. Chromel vs Alumel thermocouples in 1.6-mm-diam stainless steel sheaths were individually mated with their holes to provide uniform location of the junction. The location of the middle thermocouple lies on the desired control plane for the liquid slag-metal interface. Starting at about 6 mm below this control plane, the inside diameter of the mold tapers to a larger diameter at the bottom to readily enable withdrawal of the ingot.

The ingot withdrawal mechanism consists of a starting tab attached to a water-cooled copper bus assembly and withdrawal plate. Two electrically isolated 22-kN load cells are located in the withdrawal train. The electrical connections to the bus are equally spaced to provide a symmetrical current path. The withdrawal plate is driven by a 373-W shunt field dc motor with an external tachometer generator and solid-state electronic controller capable of remote or manual operation. A maximum withdrawal force of about 40 kN is possible with this drive mechanism. The motor is operated under speed feedback control from the tachometer in both remote and manual modes. In the remote mode, a 0 to 10-V dc signal can be sent to control the speed set point. In addition, the motor polarity can be remotely reversed. However, during operation, the withdrawal system is driven in only one direction or turned off to allow upward ingot buildup. The withdrawal system has a maximum speed of about 1.6 mm/s and is typically operated at about 0.05 to 0.1 mm/s.

The heart of the DACS is a Hewlett-Packard 9825A desktop computer with 16-bit word length and about 22K-byte read/write memory. We are currently upgrading the memory to

about 61 K bytes. The peripheral devices that are interfaced with the computer include a real-time clock, digital voltmeter, multiprogrammer for selection of input and output channels, a thermocouple uniform temperature reference (UTR), a printing terminal, a plotter, and a cartridge tape recorder.

The DACS processes input data from the following:

1. load cells (from electrode feed and ingot withdrawal),
2. resistance temperature device (from UTR),
3. thermocouples (from water cooling lines and mold wall array),
4. current shunt,
5. voltage drop from electrode to base plate, and
6. tachometer generators (from electrode feed and ingot withdrawal).

The DACS outputs the following control functions:

1. motor speed control voltages (electrode feed and ingot withdrawal),
2. flux feed on-off, and
3. weld contactor on-off.

DEVELOPMENT OF TECHNIQUE FOR LOCATION OF THE LIQUID SLAG-METAL INTERFACE

As previously discussed, we identified early in our program that the development of a technique for location of the liquid slag-metal interface was one of our most critical problems. Review of available literature indicated that the most common method involved the use of a radioactive source and detector (6,7). This system is used to detect density changes, which reflect movement of the slag-metal interface. We examined the feasibility of using a source-detection system. However, several aspects of this approach were veiwed as undesirable. The small size of our mandrel and intended use of both hollow and solid ingots resulted in the need for an external source-detector. The radiation path would have had a parallel offset from the mold centerline by about 38 mm to reduce the length. However, the resultant path still required that sections of the mold wall would have to have windows machined to reduce attenuation of the gamma rays from the proposed 3.7 GBq ^{137}Cs source. The main limitations with the use of such a system involved space restrictions, complications due to safety considerations, and cost. However, it should be noted that these

limitations were related to the physical size of our mold and available program funds. Therefore, on a larger mold we might have chosen a source-detector.

Evaluation of Ultrasonic Techniques

Our first attempt to develop an alternate interface location technique involved analysis of an ultrasonic signal passed through a continuous copper mold wall. We constructed a small ESC system with a static mold. A flat was machined on the outer surface of the mold to provide optimum transducer coupling. A 5-MHz ceramic transducer was operated in a pulse-echo mode. We attempted to detect signal velocity changes due to passage through regions of different density (i.e., liquid slag vs metal). However, the complex mold-slag skin interface caused too much signal attenuation to enable analysis (8).

We next attempted to transmit a signal up through the bottom of the mold by coupling a high-temperature transducer to the starting tab. A hole was drilled in the bottom of the mold to enable the transducer to contact the starting tab. Although we experienced problems with deterioration of high-temperature couplants, the main deterrent was signal attenuation through the cast austenitic stainless steel structure. We therefore abandoned this approach.

Finite-Element Modeling of Temperature Profiles

A recent report described the use of thermocouples embedded in a static LSR mold to study heat flow (9). We performed finite-element modeling studies to determine the applicability of these techniques to our dynamic collar mold. All the finite-element computations and graphics were performed with a program called PAFEC (Programs for Automatic Finite-Element Calculations). The heat transfer analyses used two-dimensional conduction and convection in both steady-state and transient conditions. The location of the thermocouples (Fig. 2) was based upon finite-element modeling of the steady-state temperature distribution. Figure 3 shows the steady-state temperature distribution in a section of the mold wall calculated with a 46-element mesh. The following boundary conditions were used.

1. constant thermal flux at inner wall of mold (obtained from ref. 10),

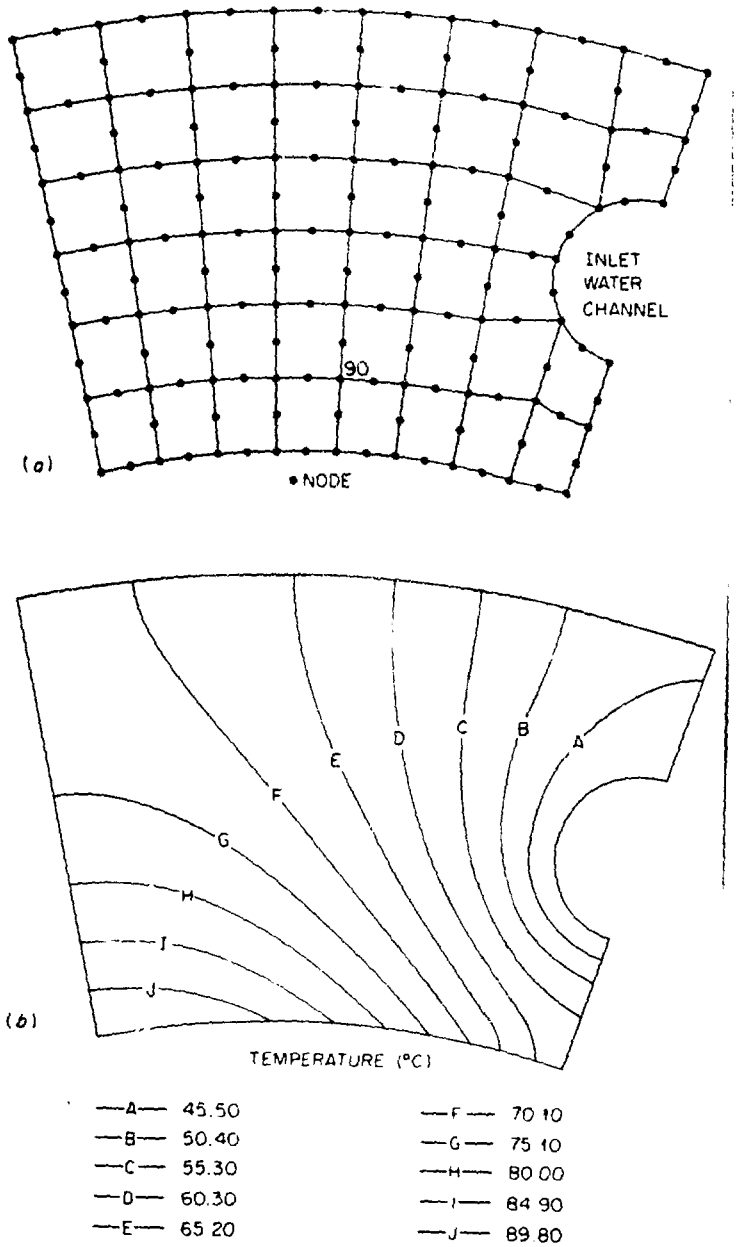

Fig. 3. Steady-State Temperature Distribution in Section of Mold Wall Calculated with 46-Element Mesh. (a) Mesh. (b) Temperature distribution.

2. constant temperature of 40°C at cooling channel wall (higher temperature than the usual water temperature was used to account for the heat transfer coefficient),
3. outer wall of mold insulated,
4. radial cuts on mesh with symmetrical insulated boundaries, and
5. negligible heat transfer in the axial direction.

We chose to locate the thermocouples at node 90 [Fig. 3(a)]. This location had a good temperature gradient without being too close to the channel. The vertical spacing and number of thermocouples in the array were based upon the availability of input channels and those used in another study (9).

To investigate errors resulting from a coarser mesh, meshes with eight and six elements were also examined. The eight-element mesh, which had just three layers of elements in the radial direction, produced flux gradients similar to that for the 46-element mesh in the region of interest near the chosen thermocouple location. Therefore, the mesh used to evaluate the thermocouple response to transient conditions was based on the eight-element plane mesh.

To study the response of the thermocouples to a moving interface, an axisymmetric mesh with three layers in the radial direction and 20 layers in the axial direction was used. A transient linear heat transfer analysis with 100 time steps was performed. To make an axisymmetric approximation, the effect of heat removal by the cooling channels was not modeled. The following boundary conditions were therefore used:

1. axially and time-varying thermal flux at inner wall of mold (obtained from ref. 10),
2. no heat removal by cooling channels, and
3. outer wall of mold insulated.

The flux distribution was moved over the mesh at a rate of 10 mm/s for 10 s and then stopped. This was done by inputting the thermal flux at the inner mold wall as a function of time. This corresponds to a rate approximately 2 orders of magnitude greater than our typical withdrawal rate. Figure 4 compares thermal responses of the inside mold wall and a thermocouple located as previously described. These graphs show that the thermocouple temperature closely follows that of the inside mold wall for conditions of both approach and departure. It should be noted that the continued increasing temperatures in Fig. 4(a) after the flux movement is stopped results from the assumption of no heat removal by the cooling channels.

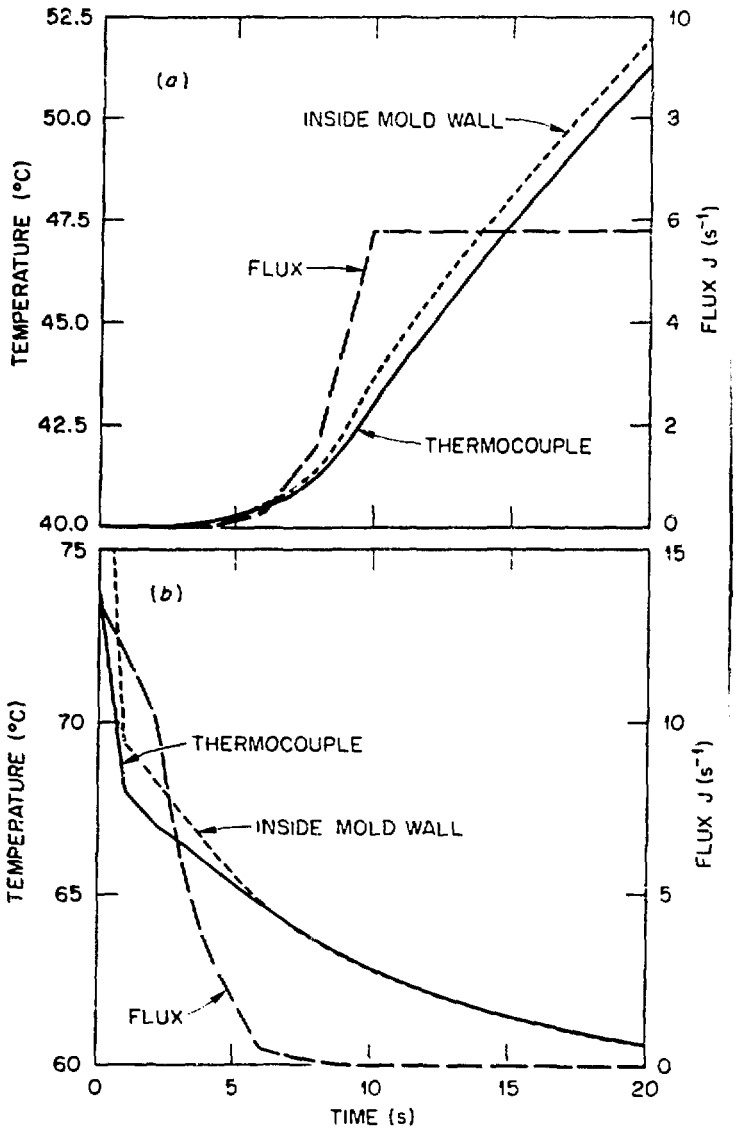

Fig. 4. Two Examples Comparing Thermal Responses of Inside Mold Wall and Thermocouple to a Heat Flux Distribution Moving at 10 mm/s for the First 10 s. (a) Response to approaching flux at location near bottom of mold, well away from original interface. (b) Response to receding flux at location near top of mold near original interface.

Development of Algorithm for Prediction Using Thermocouple Array

For determining the slag-metal interface location, we developed an algorithm based upon the predicted ability of our thermocouple location to respond to maximum transient conditions. Three algorithms were tried for determining the interface location. The primary assumption is that the interface is at the location of highest mold-wall temperature, which is at the location where the flux is maximum (9).

The first method used was a mean value algorithm. If it is assumed that the temperatures are normally distributed around the mean (Gaussian), location of the maximum temperature involves simply the computation of the moment. The algorithm is expressed as

$$X_m = \frac{T_1X_1 + T_2X_2 + T_3X_3 + T_4X_4 + T_5X_5}{(T_1 + T_2 + T_3 + T_4 + T_5)} \qquad (1)$$

where the (T,X) pairs are the temperatures T at the five thermocouple locations X.

The algorithm was coded and plots were prepared for various ingots. The locations of the maximum temperature did not appear reasonable. The data contained considerable noise or scatter and the location was predicted erratically. The temperature distribution tended to be skewed upward by convective effects in the mold. An attempt was made to filter out the noise in the data by averaging the data at several times; this was also not particularly successful.

The next method tried was to best fit a quadratic polynominal (parabola) with the least squares criterion through the five data points. The form of the equation is

$$T = C_1 + C_2X + C_3X^2 \ . \qquad (2)$$

The coefficients C_i need to be chosen such that the sum of squares of the residuals is a minimum. The problem reduces to one of solution of simultaneous linear equations and may

be particularly simplified when the sampling points (thermocouples) are in fixed locations at equal distances. The residuals are given by

$$r_n = C_1 + C_2 X_n + C_3 X_n - T_n \ . \qquad (3)$$

For the sum of squares of the residuals to be minimum we take

$$\frac{\partial}{\partial C_k} \sum_{i=1}^{n} (r_i)^2 = \sum_{i=1}^{n} r_i \frac{\partial r_i}{\partial C_k} = 0, \ k = 1, 2, 3 \ . \qquad (4)$$

This yields three simultaneous equations, which can be written in matrix form:

$$[A]\{C\} = \{T\} \ . \qquad (5)$$

For the thermocouple spacing of 50 mm, the values for the [A] matrix can routinely be developed and the matrix inverted and programmed.

This algorithm seemed to work better than the mean-value method. However, under some circumstances erratic locations of the maximum temperature would be predicted. The location of the vertex of the parabola would be shifted a great deal by one noisy temperature point. We attempted to filter out unreasonable points by not using any predictions that were, say, more than 40 mm from the thermocouple of maximum temperature. All this tended to build up the computational complexity, so a simpler approach was taken next.

The most successful algorithm attempted for location of the slag-metal interface was the fitting of a quadratic polynomial (parabola) through the point of highest temperature and the point on each side.

To simplify coding, a coordinate transformation is made. We start with five thermocouple readings $T(X_i)$. We fit the equation

$$T = A' + B'x + C'x^2 \ . \qquad (6)$$

We test the five temperatures and set $X_2 = X$ at the location of the hottest temperature. The thermocouple just above is X_1 and the one just below is X_3. We set

$$\begin{aligned} Z_1 &= X_1 - X_3 , \\ Z_2 &= X_2 - X_3 , \\ Z_3 &= X_3 - X_3 = 0, \end{aligned} \tag{7}$$

The temperatures at these three thermocouples — T_1, T_2, and T_3 — are known and are set into three equations as

$$\begin{aligned} T_1 &= A + BZ_1 + CZ_1^2 , \\ T_2 &= A + BZ_2 + CZ_2^2 , \\ T_3 &= A + BZ_3 + CZ_3^2 = A . \end{aligned} \tag{8}$$

The first two of the above equations may be combined with the third to give

$$\begin{aligned} T_1 - T_3 &= BZ_1 + CZ_1^2 , \\ T_2 - T_3 &= BZ_2 + CZ_2^2 . \end{aligned} \tag{9}$$

The constants B and C can be written as

$$\begin{aligned} C &= [Z_2(T_1 - T_3) - Z_1(T_2 - T_3)]/(Z_2Z_1^2 - Z_1Z_2^2) , \\ B &= (T_1 - T_3)/Z_1 - CZ_1 . \end{aligned} \tag{10}$$

The location of the maximum temperature, which is the assumed location of the slag-metal interface, is where the gradient vanishes, or

$$\frac{\partial T}{\partial Z} = 0 = B + 2CZ . \tag{11}$$

Thus $Z_m = -B/2C$ at the maximum temperature, which is given by

$$T_m = T_3 + BZ_m + CZ_m^2 . \qquad (12)$$

Transformation back from the Z-coordinate to other coordinates is easily accomplished by setting

$$X = Z + X_3 , \qquad (13)$$

where X_3 is the coordinate of the thermocouple previously described.

During verification of the ability of this algorithm to predict the interface location, we encountered errors due to erroneous thermocouple readings. Attempts at filtering the data caused undesirable location prediction responses. The best solution was a double reading technique, whereby the thermocouples were read twice and the readings rejected if they differed by more than 2%. We verified predicted interface locations by stopping withdrawal above and below the control plane (middle thermocouple) and allowing the ingot to cool down. The solidified slag cap was then removed and the location of the ingot top was measured. Table 1 compares predicted versus measured interface locations. These values are based on a coordinate system in which the middle thermocouple is the zero plane, with positive values above and negative values below. The results indicate a good ability to locate the interface with this technique.

Table 1. Comparison of Predicted and Measured Slag-Metal Interface Locations

Ingot	Final Interface Location, mm	
	Predicted	Measured
IN-50	34	35.3
IN-52	−12.1	−9.7
IN-53	−2.9	−2.2

DESCRIPTION OF CONTROL PROGRAM

Operation of our system is controlled by a software program using a Hewlett-Packard high-level language called HPL. The program has three modes of operation: start, run, and stop. We currently use a cold starting technique in the start mode. An electrode with a conical end initially contacts the starting tab and is withdrawn after the power is applied, thereby establishing an arc. The electrode end is surrounded by granulated slag. We are currently using a 70% CaF_2–15% CaO–15% Al_2O_3 slag to melt type 316 stainless steel electrodes. The voltage is read at 0.1-s intervals and is used to provide feedback control to the electrode drive mechanism to maintain constant voltage during arcing. Once sufficient slag is melted and resistance heating begins, the system is switched to the run mode. Although we are currently using a cold start technique for solid ingots, it will be necessary to develop hot start capability for hollow ingots.

In the run mode data are read at two intervals. Voltage is read at 2-s intervals and used to provide feedback control to the electrode drive mechanism. The remaining data are read at 10-s intervals, used by controlling subprograms, and printed for operator review, as shown in Fig. 5 for the first few minutes of a run. In addition, the interface location is continuously plotted, as shown in Fig. 6. Our data are maintained in a 30-element array in memory, with the entire array being recorded on a tape cartridge every 600 s.

Control of system voltage is currently used instead of electrode immersion control (11). The current varies as a function of the voltage-amperage characteristic of our power supplies. The feedback control for the electrode drive mechanism consists of a simple step speed command. If the voltage is greater or less than the set point, the electrode feed direction is appropriately set and speed is momentarily increased and then returned to a set rate. Figure 5 (column 16) shows how closely voltage was controlled for a set point of 13 V. The electrode feed rate can be manually increased or decreased by the operator during the run. Our future system will use current and electrode immersion control (11).

The location of the slag-metal interface [Fig. 5 (column 19)] is determined from the mold wall temperatures (columns 1–5) as previously discussed. In our case, this

1	2	3	4	5	6	7	8	9	10	11
				TEMPERATURE,C						
MOLD TOP	MOLD	MOLD	MOLD	MOLD BOT	IW-1	MWC1	MWC2	MWC3	M/PW	SW-1
9.7	10.7	13.2	10.6	9.0	8.4	9.1	9.6	9.7	8.9	8.4
9.9	11.6	15.0	11.4	9.6	8.3	9.2	10.0	10.2	8.8	8.3
10.4	12.7	17.4	12.6	10.0	8.3	9.5	10.3	10.5	8.9	8.4
11.0	13.9	21.0	14.8	10.9	8.5	10.0	10.9	11.6	8.7	8.6
12.2	16.5	29.3	17.8	11.8	8.3	10.4	11.4	12.7	9.2	8.6
13.0	18.6	35.4	20.3	13.0	8.5	11.0	12.4	13.2	9.3	8.6
14.0	20.7	40.8	22.6	13.6	8.1	11.4	12.8	13.6	9.3	8.6
15.0	22.6	45.5	25.1	14.8	8.4	11.8	13.2	14.0	9.4	8.6
15.7	24.1	48.6	26.5	15.2	8.1	12.1	13.4	14.4	9.5	8.6
16.4	25.1	51.7	28.1	16.1	8.4	12.4	13.7	14.7	9.6	8.6
17.0	26.4	54.4	29.3	16.7	8.4	12.6	13.9	14.9	9.7	8.6
17.7	27.6	57.2	30.6	17.2	8.4	12.9	14.0	15.1	9.7	8.6
18.2	28.8	59.8	31.6	17.4	8.1	13.2	14.3	15.2	9.9	8.7
18.7	29.8	62.1	32.7	17.9	8.3	13.2	14.3	15.2	9.6	8.7
19.2	31.0	64.2	33.6	18.6	8.5	13.7	14.5	15.4	10.0	8.7
19.7	31.9	65.6	34.5	18.6	8.3	13.7	14.3	15.1	10.2	8.7
20.0	32.8	66.9	35.2	19.0	8.3	13.9	14.2	15.5	10.1	8.7
20.6	33.6	69.4	35.9	19.3	8.1	14.2	14.7	15.5	10.2	8.7
21.2	34.7	69.5	36.5	19.9	8.5	14.4	14.8	15.6	10.3	8.7
21.3	35.1	69.8	36.9	19.8	8.5	14.5	14.9	15.7	10.3	8.8
21.7	36.0	71.1	37.4	19.9	8.3	14.5	14.8	15.9	10.4	8.9
22.2	36.8	72.1	37.7	20.2	8.2	14.7	15.2	15.9	10.6	8.9
22.6	37.9	72.8	38.2	20.2	8.4	14.8	15.2	15.9	10.3	8.9
23.2	38.3	73.1	38.4	20.3	8.4	14.7	15.2	15.8	10.2	8.9
23.4	39.0	72.5	38.4	20.3	8.4	14.8	15.1	16.1	10.7	9.0
23.8	39.6	72.9	38.9	20.4	8.2	15.0	15.5	16.2	10.7	8.9
24.0	40.4	73.3	39.6	20.7	8.2	15.1	15.6	16.3	10.7	8.9
24.5	41.6	73.9	40.3	21.0	8.5	15.2	15.7	16.3	10.6	9.0
24.9	42.5	74.4	40.6	21.4	8.5	15.3	15.9	16.3	10.7	9.0
25.6	43.6	74.3	40.7	21.2	8.4	15.2	15.7	16.3	10.8	9.0
26.2	44.5	74.3	40.7	21.3	8.2	15.4	16.1	16.3	10.7	9.0
26.6	45.1	74.2	40.8	21.2	8.3	15.2	15.7	16.1	10.7	8.9

1–5 MOLD TEMPERATURES, °C
6 INLET WATER TEMPERATURE, °C
7–9 MOLD COOLING WATER OUTLET TEMPERATURES,°C
10 WITHDRAWAL ASSEMBLY COOLING WATER TEMPERATURE, °C
11 ELECTRODE HOLDER COOLING WATER TEMPERATURE, °C

Fig. 5. Typical Data Printout for Beginning Portion of an ESC Run for a Solid Ingot.

12	13	14	15	16	17	18	19	20
ELECT Wt Kg	MELT RATE Kg/Hr	INGOT LOAD Kg	AMPS	VOLT	FEED RATE mm/m	WITH RATE mm/m	S/M LOC mm	TIME Sec
-3.65	0.00	-1	1120	15.7	7.1	2.5	1.1	0
-5.23	0.00	23	1064	14.7	7.2	2.5	2.9	10
-1.09	0.00	40	1080	16.0	7.3	3.0	1.1	20
12.55	0.00	72	1264	15.1	7.2	0.0	-4.6	30
15.67	0.00	69	1464	14.2	7.1	0.0	-3.9	50
15.00	0.00	68	1576	12.9	7.1	0.0	-3.9	60
21.34	0.00	68	1744	12.6	7.1	0.0	-3.7	70
17.26	0.00	66	1680	12.7	7.1	0.0	-4.4	80
11.69	0.00	65	1616	13.1	7.2	0.0	-4.0	90
20.30	0.00	65	1664	13.0	7.0	0.0	-4.5	100
3.94	0.00	63	1520	13.1	7.1	0.0	-4.1	110
20.83	0.00	65	1672	12.5	7.0	0.0	-4.0	120
4.81	0.00	63	1696	13.0	7.1	0.0	-3.6	130
20.85	0.00	63	1568	13.4	7.2	0.0	-3.6	140
13.04	0.00	62	1624	12.3	7.1	0.0	-3.1	150
22.78	0.00	63	1680	13.0	7.0	0.0	-3.0	160
16.63	0.00	62	1624	13.0	7.2	0.0	-2.7	170
16.97	0.00	61	1608	12.9	7.1	0.0	-2.5	180
17.11	0.00	61	1640	12.5	7.2	0.0	-2.0	190
18.39	0.00	61	1624	13.1	7.3	0.0	-2.0	200
19.48	0.00	61	1656	13.3	6.9	0.0	-1.6	210
22.12	0.00	60	1584	13.1	7.0	0.0	-0.9	220
21.14	0.00	60	1624	12.9	7.2	0.0	-0.4	230
21.95	0.00	60	1600	13.1	7.1	0.0	-0.1	240
23.14	0.00	59	1640	13.5	7.1	0.1	0.6	250
21.19	0.00	74	1592	13.5	7.2	1.5	0.8	260
21.44	.00	92	1616	13.2	7.2	1.5	0.9	270
23.22	.00	113	1616	12.2	7.0	1.7	1.5	280
23.04	0.	135	1792	13.0	7.0	2.5	2.2	290
23.35	0.00	160	1832	12.2	7.1	3.3	3.3	300
23.40	0.00	196	1600	11.7	7.2	4.6	4.5	310
24.85	0.00	231	1584	13.4	7.1	5.9	5.1	320

12 ELECTRODE MASS, kg
13 MELT RATE, kg/h
14 WITHDRAWAL MASS, kg
15 CURRENT, A
16 POTENTIAL DROP, V
17 ELECTRODE FEED RATE, mm/min
18 INGOT WITHDRAWAL RATE, mm/min
19 SLAG-METAL INTERFACE LOCATION, mm
20 TIME, s

Fig. 5 (Cont.)

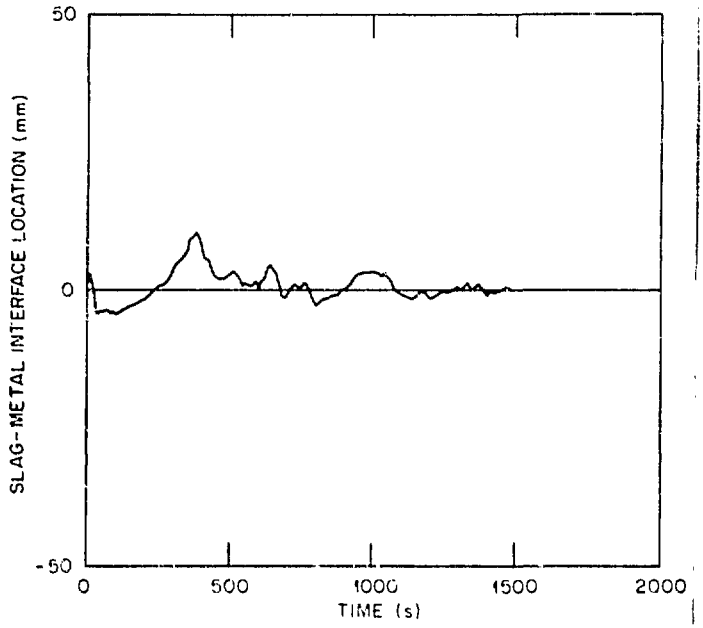

Fig. 6. Variation of Slag-Metal Interface Location During Run With Initial Data Shown in Fig. 5.

location becomes the error function, $e(t)$, in the control law for a proportional-integral-derivative three-mode controller defined by

$$M(t) = K_1 e(t) + K_2 \int_0^t e(t)\, dt + K_3 \frac{de(t)}{dt} , \qquad (14)$$

where $M(t)$ = manipulated variable (ingot withdrawal speed),

$e(t)$ = error (interface location),

K_1 = proportional constant,

K_2 = integral constant,

K_3 = derivative constant.

Figure 6 demonstrates our control capability using $K_1 = 0.15$, $K_2 = 0.01$, and $K_3 = 10$. At the beginning of each run we typically see a few erroneous interface locations. These locations are always positive and cause the controller

to increase ingot withdrawal [Fig. 5 (column 18)], thereby lowering the interface. These erroneous locations occur because the mold temperature profile has not reached equilibrium. However, this situation does not appear to be a problem since our most critical hollow casting operation will be more concerned with raising the interface location. As shown in Fig. 5 (column 18), once the interface drops below the control plane, the ingot withdrawal is stopped. Figure 6 shows that after the initial perturbations are damped out we are able to accurately control the interface location.

The ingot withdrawal load [Fig. 5 (column 14)] will also be used in the withdrawal control system for casting hollow ingots, as previously reported (7). This load will provide an overcheck capability if a failure occurs in the interface location algorithm. The overcheck system would respond to a load exceeding a predetermined set point by increasing the withdrawal rate.

We currently monitor but do not control melt rate. The melt rate [Fig. 5 (column 13)] is determined from the changing weight of the electrode [Fig. 5 (column 12)]. The melt rate is shown as zero because we do not determine it until after 420 s, as will be explained later. From our initial experiences and those reported by others, we found that a large number of electrode weight measurements were needed to determine the rate of change (12). This is due to various reported errors such as acceleration or deceleration of the drive system or magnetic and flotation forces acting on the tip of the electrode (12). Our low melt rate (typically 15–20 kg/h) further complicates the situation because such small weight changes are often less than the potential error. The higher melt rate capability that we will have with our new power supply should somewhat improve the situation. We attempt to reduce some of the problems by using a smaller capacity load cell with higher resolution.

The melt rate is currently determined by a linear regression analysis of 30 weight readings (300 s of data). We begin determining the melt rate after 420 s and therefore report a zero value until then as shown in Fig. 5 (column 13). Because only the most recent 30 readings are used in the analysis, the perturbations in the first 120 s of the run [Fig. 5 (column 12)] are avoided.

CONCLUSIONS

We have described the development of a system for control of electroslag casting in a collar mold. This control system has been optimized within the constraints of our existing equipment. The development of the algorithm to locate the liquid slag-metal interface by using embedded thermocouples has provided a simple and accurate solution to one of our most critical control problems. We realize that additional controls and equipment modifications will be required to properly investigate ESC transitions between austenitic stainless steels and ferritic steels. However, the demonstrated capability and flexibility of our system indicate that addtional controls should be readily implemented.

ACKNOWLEDGMENTS

We would like to acknowledge L. Adler, Ohio State University (formerly with the University of Tennessee), for performing the ultrasonic evaluations, W. Hoyle for design of the furnace, R. F. Stone and his electricians for their work on the control and power systems, V. T. Houchin for various ideas concerning equipment design, K. H. Luk and D. M. Kroeger for reviewing, S. Peterson for editing, and S. G. Frykman for preparing this manuscript.

REFERENCES

(1) E. M. Lose and A. Hogg, "Application of ESR to Alloy-Steel Forgings," *Electroslag Refining*, The Iron and Steel Institute, London, 1973, pp. 68–79.

(2) B. I. Medovar et al., "Features of the Structure of Hollow Electroslag-Melted Ingots," *Steel in the USSR*, Vol. 4, No. 1, January 1974, pp. 39–41.

(3) A. Ujiee et al., "Development of New Dynamic Casting for Application of Cylindrical Products," *Proceedings of the 14th International Symposium on ESR*, Japan Iron and Steel Institute, Tokyo, 1973, pp. 168–82.

(4) G. Hoyle, "Production of Small Ingots and Hollows by ESR," *Electroslag Refining*, The Iron and Steel Institute, London, 1973, pp. 136–44.

(5) W. E. Duckworth and G. Hoyle, *Electro-Slag Refining*, Chapman and Hall Ltd., London, 1969.

(6) A. Ujiie, *Method and Apparatus for Manufacture of Tubular Bodies by Electroslag Remelting*, U. S. Patent 3,834,443 (Sept. 10, 1974).

(7) H. J. Klein et al., *Production of Electroslag Remelted Hollow Ingots*, Stellite R&D Department of Cabot Corporation, Report 9045, September 1976.

(8) G. Hoyle, "Surface Phenomena in ESR," *Proceedings of the Sixth International Vacuum Metallurgy Conference on Special Melting*, American Vacuum Society, New York, April 1979, pp. 624–40.

(9) D. N. Pocklington and B. Patrick, "Heat Flow in 3-Phase ESR Slab Production," *Metall. Trans. B*, Vol. 10, 1979, pp. 359–66.

(10) S. Joshi and A. Mitchell, "Heat Flow in the Electroslag Process," *Proceedings of the Third International Symposium on ESR*, Carnegie-Mellon University, Pittsburgh, Part 1, 1971, pp. 27–52.

(11) F. W. Thomas, *Apparatus for Regulating the Immersion Depth of Electrodes in Electrode-Melting Furnaces*, U. S. Patent 4,075,414 (Feb. 21, 1978).

(12) R. J. Roberts, "A System for the Automatic Measurement and Control of Melt Rate During Electroslag Remelting," *Proceedings of the Fifth International Symposium on Electroslag Remelting Processes and Other Special Melting Technologies*, American Vacuum Society, New York, pp. 425–32.